THE JOURNAL OF PHYSICAL CHEMISTRY C
A JOURNAL OF THE AMERICAN CHEMICAL SOCIETY

pubs.acs.org/JPCC

Article

Wavelength Dependence of Plasmon-Induced Vibrational Energy Transfer in Fluorophore−Plasmonic Systems

Published as part of The Journal of Physical Chemistry C virtual special issue "Celebrating 50 Years of Surface Enhanced Spectroscopy".

Gerrit N. Christenson, Ziwei Yu, and Renee R. Frontiera*

Cite This: J. Phys. Chem. C 2024, 128, 10784−10789

Read Online

ACCESS | Metrics & More | Article Recommendations | Supporting Information

ABSTRACT: Understanding, predicting, and controlling plasmon−molecule energy transfer are important for improvements to plasmonic photocatalysis and photothermal therapies. Here, we use continuous wave surface-enhanced anti-Stokes and Stokes Raman spectroscopy to quantify the vibrational kinetic energy, equivalent to a molecular temperature under a Boltzmann approximation, of Raman-active vibrational modes of molecules at plasmonic interfaces. In previous work from our group, we observed an anomalous steady-state reduction in vibrational kinetic energies in benzenethiols absorbed onto the surface of gold nanoparticles. To further explore this effect, here, we quantify the wavelength dependence of vibrational energy in plasmon−fluorophore systems, where molecules can undergo electronic transitions with resonant excitation. We used three excitation wavelengths and three molecules with varying electronic resonance energies. We observe wavelength-dependent vibrational energy distributions, which we attribute to competing effects of on-resonance heating and off-resonance decrease in the population ratio. This work thus quantifies the resonance wavelength dependence of vibrational energy in plasmon molecular systems and helps to suggest future applications of tailored systems with controllable energy transfer pathways.

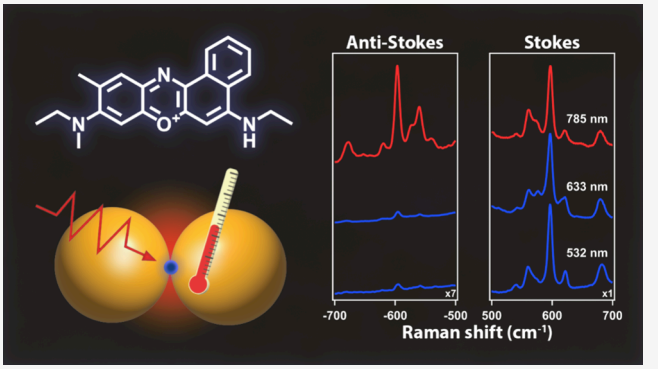

INTRODUCTION

Plasmonic materials are a class of metal and metal-like nanomaterials that are characterized by their large optical cross-sections and localized electric field enhancements.[1−5] These desirable characteristics make them ideally suited for applications, such as plasmonic photocatalysis and photothermal therapy. However, in order to optimize a specific plasmonic nanomaterial for a specific molecular interaction, we need to understand the fundamental pathways of energy flow in plasmon−molecule systems. Numerous pathways involving the flow of energy and charge have been studied with plasmonic materials,[6−11] with applications relevant to photocatalysis[16,17] and spectroscopic sensing.[12−15]

To make plasmonic photocatalysis commercially viable, better guidelines for the design and optimization of selective plasmon−molecule interactions are necessary. To further understand relevant energy transfer processes in this regime, we used Raman thermometry to prove vibrational kinetic energy distributions in proximal molecular adsorbates. The intensities of anti-Stokes and Stokes Raman scattering are proportional to the population at excited vibrational and ground vibrational states, respectively. Taking the ratio of these intensities allows for quantification of the ensemble-averaged vibrational kinetic energy of the molecular systems, in an approach termed Raman thermometry.[18−20] In plasmonics, Raman thermometry has proven itself as an effective tool to understand photothermal effects in plasmonic catalysts,[23,24] probe charge transfer of methylene blue on silver nanoparticles by studying excitation-dependent anti-Stokes Raman intensities,[21] and uncover the mechanism of plasmon-driven dimerization.[22]

Previous work in our lab showed a surprising reduction in the anti-Stokes to Stokes Raman scattering ratio under certain steady-state conditions, equivalent to molecular cooling.[25] This initial work focused on aromatic thiolated molecules bound to a range of plasmonic substrates in various solvating conditions and laser excitation wavelengths. Under 633 nm excitation, the

Received: February 21, 2024
Revised: June 7, 2024
Accepted: June 7, 2024
Published: June 18, 2024

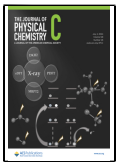

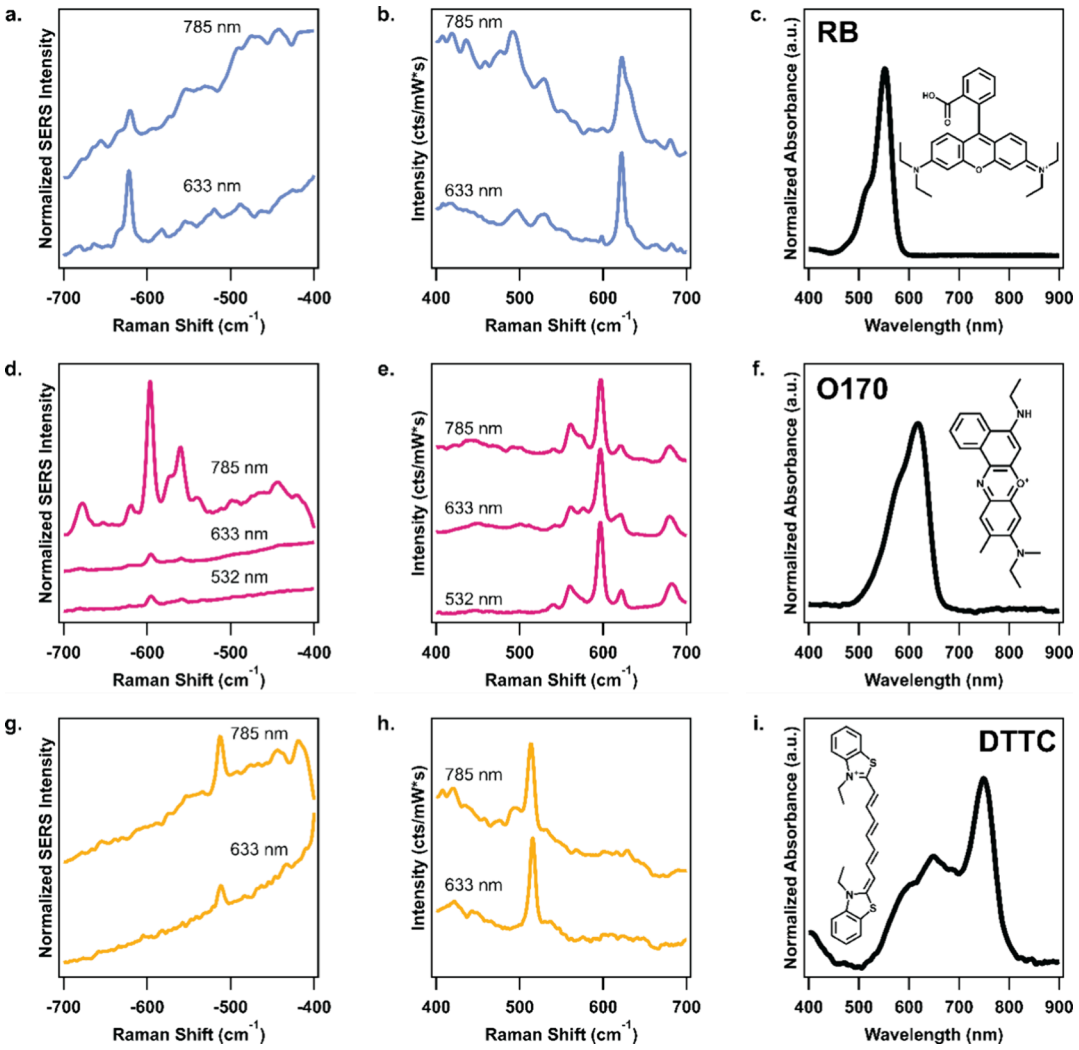

Figure 1. Surface-enhanced anti-Stokes and Stokes Raman spectra for rhodamine B (a, b), oxazine 170 (d, e), and 3,3′-diethylthiatricarbocyanine (g, h), respectively. The indicated wavelengths represent the laser excitation wavelength. We also show the molecule structure and absorbance spectra for rhodamine B (c), oxazine 170 (f), and 3,3′-diethylthiatricarbocyanine (i) dissolved in Milli-Q water.

authors found that all molecules experienced a decrease in the population ratio regardless of solvent and the plasmon resonance spectrum of the substrate. These results were attributed to either true molecular cooling caused by plasmon−molecule interactions or by undetermined differences in SERS, surface-enhanced Raman spectroscopy, out-coupling efficiencies on the Stokes and anti-Stokes sides. These past findings merit further investigation, and here, we extend this work to probe the effects of molecular electronic resonance on the vibrational kinetic energy distributions.

RESULTS

Our SERS substrates for these experiments consist of approximately 80 nm citrate-capped gold nanospheres supported on cellulose (filter paper) substrates. The structure of the filter paper supports the aggregation of gold nanoparticles into dimers, trimers, and higher-order aggregates, facilitating the formation of a heterogeneous distribution of hot spots. Our SERS measurements probe the plasmonic−molecular interactions in these most active hot spots.[26] These substrates are deliberately highly heterogeneous in an attempt to adequately sample all relevant interactions as well as to mimic realistic catalysts that would need to be manufactured on scales larger than easily possible with lithographic approaches.

For this study, we use rhodamine B (RB), oxazine 170 (O170), and 3,3′-diethylthiatricarbocyanine (DTTC) as our analyte molecules, which have different absorbance spectra, as shown in Figure 1. In particular, their absorption maxima fall close to commercially available laser wavelengths of 532, 633, and 785 nm, which are the excitation wavelengths we use in this study. We note that adsorption to plasmonic surfaces is known to shift molecular resonances by several tens or even hundreds of meV, depending on the strength of the interaction.[27−30] Further, we selected molecules that are unlikely to undergo significant plasmon-driven chemical reactions, as verified by the lack of changes in Raman spectra throughout the measurement.

Since temperature is a physical quantity used to characterize equilibrated systems, we instead report the population ratios, given that these systems are not at equilibrium. Population ratios are equivalent to the molecular vibrational kinetic energy and can be converted directly to temperatures via a form of a Boltzmann distribution, as shown in eq 1.

https://doi.org/10.1021/acs.jpcc.4c01142
J. Phys. Chem. C 2024, 128, 10784−10789

$$\text{Temperature(K)} = \frac{-\text{Energy of Vibration(J)}}{k_b \times \ln\left(\frac{\text{Intensity}_{\text{anti-Stokes}}}{C \times \text{Intensity}_{\text{Stokes}}}\right)} \quad (1)$$

where C equals $(\omega_{\text{anti-Stokes}}/\omega_{\text{Stokes}})^3$, a normalization factor that describes the wavelength dependence of the Raman scattering cross-section. We use a cubic relationship since we are comparing Stokes and anti-Stokes intensities with the same excitation wavelength, as previously described by Yu et al.[25] We define the anti-Stokes and Stokes intensities, as shown in eqs 2 and 3, respectively.

$$\text{Intensity}_{\text{anti-Stokes}} = \frac{\text{Vibration Mode Peak Area}_{\text{anti-Stokes}}}{\text{Detector Response} \times \text{Extinction}_{\omega_L+\omega_{vib}}} \quad (2)$$

$$\text{Intensity}_{\text{Stokes}} = \frac{\text{Vibration Mode Peak Area}_{\text{Stokes}}}{\text{Detector Response} \times \text{Extinction}_{\omega_L-\omega_{vib}}} \quad (3)$$

where we determine the extinction coefficients for the anti-Stokes and Stokes wavelengths by measuring the extinction spectrum of the same substrate used for SERS measurements and the detector response using toluene, cyclohexane, and chloroform as standards. Thus, we define the population ratio as shown in eq 4.

$$\text{Population Ratio} = \frac{\text{Intensity}_{\text{anti-Stokes}}}{C \times \text{Intensity}_{\text{Stokes}}} \quad (4)$$

In Figure 1, we show the anti-Stokes and Stokes spectra for RB (Figure 1a,b), O170 (Figure 1d,e), and DTTC (Figure 1g,h). Further, we show the molecular absorbance of RB (Figure 1c), O170 (Figure 1f), and DTTC (Figure 1i) in Milli-Q water. For visual comparison, we normalize all the Stokes spectra to the same intensity. Qualitatively, we can see that the anti-Stokes signal intensity varies immensely for different excitation wavelengths. For RB, the 785 nm excitation has a much lower anti-Stokes intensity compared to its 633 nm excitation. Additionally, we observe that the 622 cm^{-1} mode of RB broadens by 8 cm^{-1} when comparing 633 to 785 nm excitation. For O170, the 785 nm excitation has a much higher anti-Stokes signal intensity when compared to the 633 and 532 nm excitations. For DTTC, both the 785 and 633 nm excitations have lower intensity anti-Stokes signals, with the 785 nm excitation being slightly higher in anti-Stokes intensity compared to the 633 nm excitation. We cannot obtain 532 nm excitation data for RB and DTTC because of bulk solution molecular fluorescence from unabsorbed molecules in the sample matrix. In particular, for RB, the fluorescence intensity saturates our detector in the 500 nM−5 μM concentration range, which is near the detection limit for SERS.[31−33] For DTTC, we similarly see a broad and intense fluorescence background in our Raman spectra.[34] This likely results from the formation of H-aggregates, which cause a blue shift in the fluorescence of the molecules, as previously observed in a similar system.[35,36]

In Figure 2, we show the molecular absorbance of RB (Figure 2a), O170 (Figure 2b), and DTTC (Figure 2c) in aqueous solution overlaid with the population ratios determined from our Raman thermometry analysis. For RB, O170, and DTTC, we show the 622, 597, and 515 cm^{-1} modes, respectively. We obtain the error bars from triplicate measurements and report a 90% confidence interval. We express the data in this manner to facilitate a direct comparison of the solvated molecular electronic transition energies with the wavelength-dependent SERS population ratios. A clear and distinct wavelength-dependent population ratio occurs in RB, O170, and DTTC. For RB, we observe a population ratio increase at 633 nm excitation and a decrease at 785 nm excitation. For O170, we observe a population ratio decrease at 532 and 633 nm excitation (on-resonance) and an increase at 785 nm excitation (off-resonance). For DTTC, we observe a population ratio decrease at 633 and 785 nm excitation, both of which are on-resonance wavelengths.

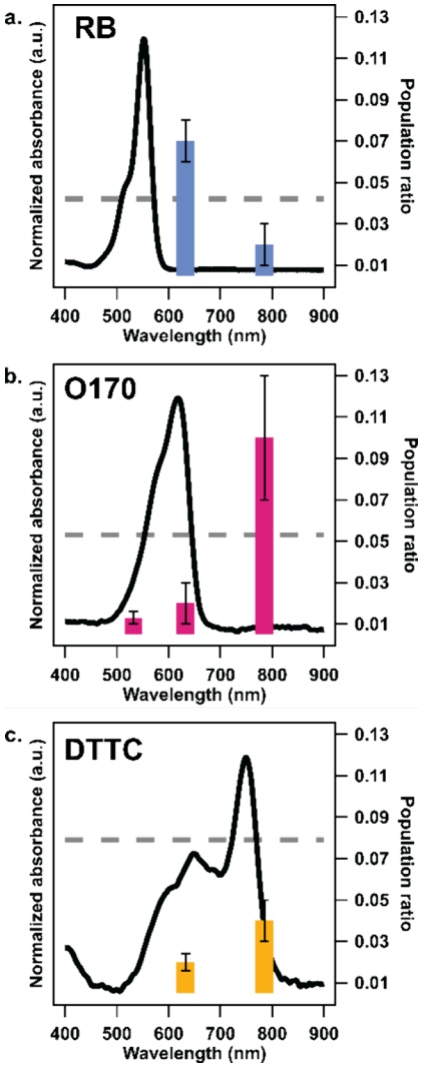

Figure 2. Absorbance spectra overlapped with the population ratios at each excitation wavelength for RB (a), O170 (b), and DTTC (c). RB and O170 are 5 μM in water, and DTTC is sparingly soluble in water. The gray dotted line represents room temperature population ratios for each vibrational mode.

In Table 1, we show the results of our Boltzmann analysis of our population ratios for RB, O170, and DTTC at the 622, 597, and 515 cm^{-1} modes, respectively. We collect spectra for multiple powers for excitation wavelength, where the 532, 633, and 785 nm lasers achieve 5, 8, and 37 mW maximum power at the sample, respectively. For comparison, we use 5 mW power as the standard across each excitation source to account for the detector's wavelength-dependent response. We obtain the

https://doi.org/10.1021/acs.jpcc.4c01142
J. Phys. Chem. C 2024, 128, 10784−10789

Table 1. Population Ratios of Various Fluorophores as a Function of the Wavelength and Laser Power[a]

		molecule		
		RB	O170	DTTC
wavelength	power	population ratios		
532 nm	5 mW		0.013 ± 0.003	
633 nm	5 mW	0.07 ± 0.01	0.02 ± 0.01	0.020 ± 0.004
	8 mW	0.11 ± 0.02	0.015 ± 0.002	0.020 ± 0.002
785 nm	5 mW	0.02 ± 0.01	0.10 ± 0.03	0.04 ± 0.01
	8 mW	0.02 ± 0.01	0.10 ± 0.05	0.03 ± 0.01
	37 mW	0.03 ± 0.03	0.12 ± 0.04	0.03 ± 0.03

[a]The absorption maxima for RB, O170, and DTTC are 546, 624, and 765 nm, respectively. The Raman modes used for our thermometry analysis for RB, O170, and DTTC are 622, 597, and 515 cm^{-1}, respectively.

error for each value by taking the measurements in triplicate and using a 90% confidence interval. We note that the population ratios for a given molecule at a given excitation wavelength are similar for all of the measured modes.

DISCUSSION

Upon further inspection of Figure 2, we see a general trend when comparing the absorption spectrum of the molecules in solution and the wavelength-dependent population ratios with one exception. When the excitation wavelength is in resonance with the absorption, we typically see a decrease in the vibrational population ratio. For O170 and DTTC, off-resonant excitation results in an increase in the population ratio. For RB, we similarly see an increase in the population ratio for the off-resonant 633 nm excitation, but for the 785 nm off-resonant excitation, we observe a decrease in the population ratio, the only data point that does not match the general trend.

We selected molecular absorbates that weakly bind to the surface of the gold nanoparticles. This is done such that the HUMO−LUMO energy gaps of the absorbates likely do not change by more than 100 nm upon adsorption, which is less than the energy difference between our excitation sources.[37,38] While it is challenging to determine molecular electronic transitions on a highly heterogeneous plasmonic surface with a vast range of possible adsorption geometries, the nature of the molecule−plasmon interaction and the lack of significant changes in Raman frequencies upon adsorption support our use of solution-based absorption measurements as an estimate for molecular electronic transitions.

With the exception of 785 nm excitation of RB, we observe a suppression of vibrational population ratios when exciting on resonance with molecular electronic transitions and an increase in the vibrational population ratios when exciting off resonance. The off-resonance behavior is likely explained by photoinduced heating of the plasmonic surface, as has been well-established for photothermal therapy applications[39] as well as in ultrafast SERS measurements.[22] However, the on-resonance behavior is more surprising, given that in this regime, the molecules are more likely to directly adsorb and be involved in resonant energy transfer processes. Regardless, these results are similar to our previously published work, which showed suppression of excited vibrational state populations in benzenethiol derivatives on gold surfaces when excited with visible wavelengths. In that work, we proposed that resonant conditions could lead to charge transfer between the metal and adsorbed molecules, which would result in a reduction of vibrational excited states. Such a charge transfer process would need to be endothermic, and as such, the depopulation of the vibrational energy levels provides the necessary energy to facilitate the charge transfer process, resulting in the observed population ratio decrease. A similar mechanism may be involved here, and this work provides additional support for the resonance conditions required for such charge transfer to occur.

The exception to the general trend of population ratio decrease with on-resonance excitation is with the 785 nm excitation of RB, and we attribute this to an adsorption-induced change in the electronic resonance. Inspection of the higher frequency modes of the Raman spectrum for RB at 785 nm excitation compared to 633 nm excitation shows new peaks, specifically at 993 and 1103 cm^{-1}. The full 633 and 785 nm spectra for RB, which include the higher frequency modes, are given in the Supporting Information in Figure S4. Further, the peaks are significantly broadened in the 785 nm measurement compared to the 633 nm measurement. This is apparent for the 622 cm^{-1} Raman-active mode during the 785 nm excitation, which is the mode we use for the thermometry analysis of RB. The peak shoulder is red-shifted by approximately 8 cm^{-1} in the 785 nm measurement compared to the 633 nm measurement. Therefore, an alternate equilibrium form of RB is either formed from the 785 nm excitation or becomes on-resonance when excited with 785 nm excitation induced from binding to the surface of the nanoparticles.[13,40] So, it is likely that RB is resonant with the 785 nm excitation and off-resonant with 633 nm excitation when absorbed to the surface of gold. This could explain why the 785 nm excitation of RB has a decrease in the population ratio, even when it is off-resonance in terms of the molecular absorbance in solution. Thus, the binding geometry of the RB would be significantly different from the structures of the free molecules in solution. As further support of the idea that changes in the molecular structure of Rhodamine B cause a shift in electronic conditions, which makes it resonant at 785 nm, we took Raman thermometry measurements of Rhodamine 6G under the same conditions (Figure S6). We observe no changes to the vibrational frequency, indicating that Rhodamine 6G should not be resonant at 785 nm. We also find that the population ratio of the 650 cm^{-1} mode is equivalent to a temperature of 370 ± 20 K, consistent with the hypothesis that off-resonant excitation results in modest heating.

Molecular binding and aggregation are known to alter the electronic structure of molecules in the condensed phase, so it is possible that RB is resonant with the 785 nm excitation and off-resonant with 633 nm excitation when absorbed onto the surface of gold. This would explain why the 785 nm excitation

https://doi.org/10.1021/acs.jpcc.4c01142
J. Phys. Chem. C 2024, 128, 10784−10789

of RB has a decrease in the population ratio, even when it is off-resonance in terms of the molecular absorbance in solution.

From our results, it seems plausible that molecular resonance has an effect on the decrease in the population ratio. We hypothesize that when molecular resonance conditions are met, we see a decrease in the population ratio. When the HOMO−LUMO electronic energy gap of the fluorophores is resonant with the LSPR, localized surface plasmon resonance, both charge transfer and plasmon-induced energy transfer could occur.[21,41−43] Both of these processes would allow for an increase in vibrational energy transfer pathways.

Due to the uncertainty in our results and the complexity of molecular-plasmonic systems, we express the need for further experiments regarding the observed phenomena. Performing similar measurements with additional excitation wavelengths would offer insight into when a decrease in the population ratio changes to an increase (and vice versa). Further, complementary computation methods to determine the molecular absorption of both thiolated molecules and fluorophores upon absorption to plasmonic substrates would help improve the certainty of our conclusions.

CONCLUSIONS

In this work, we probe the vibrational energy transfer in plasmonic fluorophore systems. To do so, we conducted SERS measurements followed by Raman thermometry analysis to obtain vibrational population ratios, a direct measurement of molecular kinetic energy. We determined that on-resonance excitation leads to a decrease in population ratios in plasmonic fluorophore systems, while off-resonance excitation leads to an increase in population ratios. The plasmonic material facilitates some energy redistribution, which uses vibrational energy for a plasmon-induced charge transfer process. The wavelength-dependent plasmon population ratio effect should be considered when designing plasmonic photocatalysis, as vibrational energy can be instrumental in the photochemical outcome of plasmon-driven chemistry. Choosing an excitation that aligns with the maximum of the plasmon resonance to drive a reaction without considering the electronic structure of the adsorbate could hinder reactivity or lead to undesired products if the reaction is dependent on the vibrational energy population.

ASSOCIATED CONTENT

Supporting Information

The Supporting Information is available free of charge at https://pubs.acs.org/doi/10.1021/acs.jpcc.4c01142.

Additional Raman spectra, UV−visible characterization, Raman instrumentation, data processing, and supporting spectra (PDF)

AUTHOR INFORMATION

Corresponding Author

Renee R. Frontiera − *Department of Chemistry, University of Minnesota, Minneapolis, Minnesota 55455, United States;* orcid.org/0000-0001-8218-7574; Email: rrf@umn.edu

Authors

Gerrit N. Christenson − *Department of Chemistry, University of Minnesota, Minneapolis, Minnesota 55455, United States*

Ziwei Yu − *Department of Chemistry, University of Minnesota, Minneapolis, Minnesota 55455, United States*

Complete contact information is available at: https://pubs.acs.org/10.1021/acs.jpcc.4c01142

Notes

The authors declare no competing financial interest.

ACKNOWLEDGMENTS

This work was supported by the MRSEC Program of the National Science Foundation under award number DMR-2011401.

REFERENCES

(1) Odom, T. W.; Schatz, G. C. Introduction to Plasmonics. *Chem. Rev.* **2011**, *111*, 3667−3668.

(2) Sharma, B.; Frontiera, R. R.; Henry, A.-I.; Ringe, E.; Van Duyne, R. P. SERS: Materials, Applications, and the Future. *Mater. Today* **2012**, *15*, 16−25.

(3) Warkentin, C. L.; Yu, Z.; Sarkar, A.; Frontiera, R. R. Decoding Chemical and Physical Processes Driving Plasmonic Photocatalysis Using Surface-Enhanced Raman Spectroscopies. *Acc. Chem. Res.* **2021**, *54*, 2457−2466.

(4) Prince, R. C.; Frontiera, R. R.; Potma, E. O. Stimulated Raman Scattering: From Bulk to Nano. *Chem. Rev.* **2017**, *117*, 5070−5094.

(5) Brooks, J. L.; Warkentin, C. L.; Saha, D.; Keller, E. L.; Frontiera, R. R. Toward a Mechanistic Understanding of Plasmon-Mediated Photocatalysis. *Nanophotonics* **2018**, *7*, 1697−1724.

(6) Anker, J. N.; Hall, W. P.; Lyandres, O.; Shah, N. C.; Zhao, J.; Van Duyne, R. P. Biosensing with Plasmonic Nanosensors. *Nat. Mater.* **2008**, *7*, 442−453.

(7) Linic, S.; Christopher, P.; Ingram, D. B. Plasmonic-Metal Nanostructures for Efficient Conversion of Solar to Chemical Energy. *Nat. Mater.* **2011**, *10*, 911−921.

(8) Twilton, J.; Le, C.; Zhang, P.; Shaw, M. H.; Evans, R. W.; MacMillan, D. W. The Merger of Transition Metal and Photocatalysis. *Nat. Rev. Chem.* **2017**, No. 1, 52 DOI: 10.1038/s41570-017-0052.

(9) Aslam, U.; Rao, V. G.; Chavez, S.; Linic, S. Catalytic Conversion of Solar to Chemical Energy on Plasmonic Metal Nanostructures. *Nature Catalysis* **2018**, *1*, 656−665.

(10) Zhang, X.; Li, X.; Zhang, D.; Su, N. Q.; Yang, W.; Everitt, H. O.; Liu, J. Product Selectivity in Plasmonic Photocatalysis for Carbon Dioxide Hydrogenation. *Nat. Commun.* **2017**, *8*, 14542 DOI: 10.1038/ncomms14542.

(11) Yu, Z.; Frontiera, R. R. Intermolecular Forces Dictate Vibrational Energy Transfer in Plasmonic−Molecule Systems. *ACS Nano* **2022**, *16*, 847−854.

(12) Haes, A. J.; Zou, S.; Zhao, J.; Schatz, G. C.; Van Duyne, R. P. Localized Surface Plasmon Resonance Spectroscopy near Molecular Resonances. *J. Am. Chem. Soc.* **2006**, *128*, 10905−10914.

(13) Zhao, J.; Jensen, L.; Sung, J.; Zou, S.; Schatz, G. C.; Van Duyne, R. P. Interaction of Plasmon and Molecular Resonances for Rhodamine 6G Adsorbed on Silver Nanoparticles. *J. Am. Chem. Soc.* **2007**, *129*, 7647−7656.

(14) Zhao, J.; Das, A.; Zhang, X.; Schatz, G. C.; Sligar, S. G.; Van Duyne, R. P. Resonance Surface Plasmon Spectroscopy: Low Molecular Weight Substrate Binding to Cytochrome P450. *J. Am. Chem. Soc.* **2006**, *128*, 11004−11005.

(15) Frontiera, R. R.; Dasgupta, J.; Mathies, R. A. Probing Interfacial Electron Transfer in Coumarin 343 Sensitized TiO2 Nanoparticles with Femtosecond Stimulated Raman. *J. Am. Chem. Soc.* **2009**, *131*, 15630−15632.

(16) Brooks, J. L.; Warkentin, C. L.; Chulhai, D. V.; Goodpaster, J. D.; Frontiera, R. R. Plasmon-Mediated Intramolecular Methyl Migration with Nanoscale Spatial Control. *ACS Nano* **2020**, *14*, 17194−17202.

(17) Swearer, D. F.; Bourgeois, B. B.; Angell, D. K.; Dionne, J. A. Advancing Plasmon-Induced Selectivity in Chemical Transformations with Optically Coupled Transmission Electron Microscopy. *Acc. Chem. Res.* **2021**, *54*, 3632−3642.
(18) Lo, H. W.; Compaan, A. Raman Measurement of Lattice Temperature during Pulsed Laser Heating of Silicon. *Phys. Rev. Lett.* **1980**, *44*, 1604−1607.
(19) Malyj, M.; Griffiths, J. E. Stokes/Anti-Stokes Raman Vibrational Temperatures: Reference Materials, Standard Lamps, and Spectrophotometric Calibrations. *Appl. Spectrosc.* **1983**, *37*, 315−333.
(20) Kip, B. J.; Meier, R. J. Determination of the Local Temperature at a Sample during Raman Experiments Using Stokes and Anti-Stokes Raman Bands. *Appl. Spectrosc.* **1990**, *44*, 707−711.
(21) Boerigter, C.; Aslam, U.; Linic, S. Mechanism of Charge Transfer from Plasmonic Nanostructures to Chemically Attached Materials. *ACS Nano* **2016**, *10*, 6108−6115.
(22) Keller, E. L.; Frontiera, R. R. Ultrafast Nanoscale Raman Thermometry Proves Heating Is Not a Primary Mechanism for Plasmon-Driven Photocatalysis. *ACS Nano* **2018**, *12*, 5848−5855.
(23) Park, S.; Yeon, G. J.; Lee, H.; Shin, H.-H.; Kim, Z. H. Self-Referenced SERS Thermometry of Molecules on a Metallic Nanostructure. *J. Phys. Chem. C* **2022**, *126*, 451−458.
(24) Shin, H.-H.; Jeong, J.; Nam, Y.; Lee, K. S.; Yeon, G. J.; Lee, H.; Lee, S. Y.; Park, S.; Park, H.; Lee, J. Y.; Kim, Z. H. Vibrationally Hot Reactants in a Plasmon-Assisted Chemical Reaction. *J. Am. Chem. Soc.* **2023**, *145*, 12264−12274.
(25) Yu, Z.; Frontiera, R. R. Ostensible Steady-State Molecular Cooling with Plasmonic Gold Nanoparticles. *ACS Nano* **2023**, *17*, 4306−4314.
(26) Fang, Y.; Seong, N.-H.; Dlott, D. D. Measurement of the Distribution of Site Enhancements in Surface-Enhanced Raman Scattering. *Science* **2008**, *321*, 388−392.
(27) Cabalo, J.; Guicheteau, J. A.; Christesen, S. Toward Understanding the Influence of Intermolecular Interactions and Molecular Orientation on the Chemical Enhancement of SERS. *J. Phys. Chem. A* **2013**, *117*, 9028−9038.
(28) You, T.; Liang, X.; Gao, Y.; Yin, P.; Guo, L.; Yang, S. A Computational Study on Surface-Enhanced Raman Spectroscopy of Para-Substituted Benzenethiol Derivatives Adsorbed on Gold Nanoclusters. *Spectrochimica Acta Part A: Molecular and Biomolecular Spectroscopy* **2016**, *152*, 278−287.
(29) Rossi, T. P.; Shegai, T.; Erhart, P.; Antosiewicz, T. J. Strong Plasmon-Molecule Coupling at the Nanoscale Revealed by First-Principles Modeling. *Nat. Commun.* **2019**, *10*, 3336 DOI: 10.1038/s41467-019-11315-5.
(30) Sample, A. D.; Guan, J.; Hu, J.; Reese, T.; Cherqui, C. R.; Park, J.-E.; Freire-Fernández, F.; Schaller, R. D.; Schatz, G. C.; Odom, T. W. Strong Coupling between Plasmons and Molecular Excitons in Metal−Organic Frameworks. *Nano Lett.* **2021**, *21*, 7775−7780.
(31) Hestand, N. J.; Spano, F. C. Expanded Theory of H- and J-Molecular Aggregates: The Effects of Vibronic Coupling and Intermolecular Charge Transfer. *Chem. Rev.* **2018**, *118*, 7069−7163.
(32) Zhao, L.; Ren, X.; Yan, X. Assembly Induced Super-Large Red-Shifted Absorption: The Burgeoning Field of Organic near-Infrared Materials. *CCS Chemistry* **2021**, *3*, 678−693.
(33) Alyami, A.; Barton, K.; Lewis, L.; Mirabile, A.; Iacopino, D. Identification of Dye Content in Colored BIC Ballpoint Pen Inks by Raman Spectroscopy and Surface-Enhanced Raman Scattering. *J. Raman Spectrosc.* **2019**, *50*, 115−126.
(34) Wang, Y.; Wang, R.; Imai, Y.; Hara, N.; Wan, X.; Nakano, T. Π-Stacked and Unstacked Aggregate Formation of 3,3′-Diethylthiatricarbocyanine Iodide, a near-Infrared Dye. *New J. Chem.* **2018**, *42*, 14713−14716.
(35) Dimitriev, O. P.; Zirzlmeier, J.; Menon, A.; Slominskii, Y.; Guldi, D. M. Exciton Dynamics in J- and H-Aggregates of a Tricarbocyanine near-Infrared Dye. *J. Phys. Chem. C* **2021**, *125*, 9855−9865.
(36) Chakraborty, S.; Debnath, P.; Dey, D.; Bhattacharjee, D.; Hussain, S. A. Formation of Fluorescent H-Aggregates of a Cyanine Dye in Ultrathin Film and Its Effect on Energy Transfer. *J. Photochem. Photobiol., A* **2014**, *293*, 57−64.
(37) Tang, Q.; Jiang, D. Comprehensive View of the Ligand−Gold Interface from First. *Chem. Mater.* **2017**, *29*, 6908−6915. Principles.
(38) Dietze, D. R.; Mathies, R. A. Molecular Orientation and Optical Properties of 3,3′-Diethylthiatricarbocyanine Iodide Adsorbed to Gold Surfaces: Consequences for Surface-Enhanced Resonance Raman Spectroscopy. *J. Phys. Chem. C* **2015**, *119*, 9980−9987.
(39) Lal, S.; Clare, S. E.; Halas, N. J. Nanoshell-Enabled Photothermal Cancer Therapy: Impending Clinical Impact. *Acc. Chem. Res.* **2008**, *41*, 1842−1851.
(40) Stratton, B.-F. C.; Pierre, A. J.; Riser, E. A.; Grinalds, N. J.; Edwards, C. W.; Wohlwend, A. M.; Bauer, J. S.; Spera, R. J.; Pferdmenges, L. S.; Griffith, K. M.; Hunter, B. W.; Bobadova-Parvanova, P.; Day, C. S.; Lundin, P. M.; Fogarty, K. H. Synthesis and Optical Characterization of a Rhodamine B Spirolactam Dimer. *J. Phys. Chem. A* **2022**, *126*, 4211−4220.
(41) Li, J.; Cushing, S. K.; Meng, F.; Senty, T. R.; Bristow, A. D.; Wu, N. Plasmon-Induced Resonance Energy Transfer for Solar Energy Conversion. *Nat. Photonics* **2015**, *9*, 601−607.
(42) Boerigter, C.; Campana, R.; Morabito, M.; Linic, S. Evidence and Implications of Direct Charge Excitation as the Dominant Mechanism in Plasmon-Mediated Photocatalysis. *Nat. Commun.* **2016**, *7*, 10545.
(43) Kale, M. J.; Avanesian, T.; Xin, H.; Yan, J.; Christopher, P. Controlling Catalytic Selectivity on Metal Nanoparticles by Direct Photoexcitation of Adsorbate−Metal Bonds. *Nano Lett.* **2014**, *14*, 5405−5412.

https://doi.org/10.1021/acs.jpcc.4c01142
J. Phys. Chem. C 2024, 128, 10784−10789